Numerical Modeling of Concrete Energy Piles using a Coupled Thermo-Hydro-Mechanical Model

Alitking Anongphouth, Pooneh Maghoul & Marolo Alfaro
Department of Civil Engineering – University of Manitoba, Winnipeg, Manitoba, Canada

ABSTRACT
Harnessing shallow geothermal energy through the use of energy piles for heating and cooling of buildings has increased in recent years. Therefore, comprehensive understanding of their energy and structural performances is vital for successful applications. This paper aims to investigate the responses of concrete energy piles under thermal and thermo-mechanical loads using a coupled thermo-hydro-mechanical (THM) model. Axisymmetric finite element models were carried out for two case studies of full-scale tests of energy piles. In general, it was found that the numerical models could capture considerably well the behavior of energy piles during cooling and heating cycles in comparison with the field data published in the literature, especially during heating. It was also found that using appropriate pile head restrained conditions is crucial in order to predict the correct behavior of the energy piles.

RÉSUMÉ
L'exploitation de l'énergie géothermique peu profonde par l'utilisation de pieux énergétiques pour la climatisation des bâtiments a augmenté ces dernières années. Par conséquent, une compréhension de leurs performances énergétiques et structurelles est essentielle pour des applications réussies. Cet article vise à étudier les réponses des pieux énergétiques en béton sous charges thermiques et thermomécaniques à l'aide d'un modèle couplé thermo-hydro-mécanique (THM). Des modèles d'éléments finis axisymétriques ont été réalisés pour deux études de cas de tests grandeur nature de pieux énergétiques. En général, il a été constaté que les modèles numériques pouvaient capturer considérablement le comportement des pieux énergétiques pendant les cycles de refroidissement et de chauffage en comparaison avec les données de terrain publiées dans la littérature, en particulier pendant le chauffage. Il a également été constaté que l'utilisation de conditions appropriées restreintes de la tête de pieu est cruciale pour prédire le bon comportement des pieux énergétiques.

1   INTRODUCTION

Fossil fuel energy is neither renewable nor clean. To reduce our reliance on this limited source of energy, researchers have been exploring sustainable alternatives. One of these is shallow geothermal energy used for heating and cooling building spaces by borehole heat exchangers coupled with heat pumps also known as the ground source heat pump system (GSHPs). The GSHPs is considered to be cost-effective in the long-term and also environmentally friendly. Where piles are used to support buildings, heat exchanger pipes can be installed inside the piles using multiple U-loops or spiral coils. Thus, additional costs of drilling and installing as well as the need for extra land for the conventional borehole heat exchangers can be eliminated. The piles, therefore, serve two functions, i.e., providing structural support and harnessing geothermal energy by exchanging heat with the surrounding ground. They are commonly known as energy piles also referred to as thermal, thermo-active, geothermal, or heat exchanger piles.

Despite many benefits, integrating heat carrier fluid pipes into structural elements has raised critical questions regarding potential adverse effects of thermal changes (or thermal loadings) on the structural and geotechnical performances of the piles. Thermo-active foundations are associated with a complex thermo-hydro-mechanical (THM) process of porous materials, and currently, comprehensive knowledge of their behavior and design guidelines remain limited. These concerns coupled with the high initial investment may be the reasons why many building owners and property developers remain skeptical and reluctant to adopt this technology. A number of researchers have been working on this particular area, experimentally and numerically, with the aim to improve the understanding of the thermal effects on the energy pile itself and on its surrounding ground. So far few full-scale energy pile tests have been carried out. To the best of the authors' knowledge, three earliest full-scale energy pile tests were carried out in Europe, i.e., in Austria (Brandl 2006), in Switzerland (Laloui et al. 2006), and in the United Kingdom (Amis et al. 2008; Bourne-Webb et al. 2009). These tests, even though performed for relatively short durations, provided essential insights into the energy pile responses to thermal and thermo-mechanical loadings.

The primary objective of this paper is to use a thermo-hydro-mechanical model implemented in a finite element software to simulate the responses of the energy piles under thermal and thermo-mechanical loadings. Numerical results are then compared with data from field instrumentation published in the literature.

2   CASE STUDIES

Two case studies of energy piles were selected for numerical modeling purposes. One is the energy pile tested at Lambeth College, London, U.K. This is referred

here as the 'London energy pile'. The other is at the Swiss Institute of Technology in Lausanne, Switzerland. This is referred as 'Lausanne energy pile'. These two case studies have distinctive features. The former is a friction pile embedded mostly in clay. The latter is an end-bearing pile socketed into sandstone bedrock. The London energy pile is a trial test pile with a diameter (D) of 0.55 m and a length (L) of 23 m, and was installed through three layers of soils as given in Table 1. The Lausanne energy pile is a working pile located along the side of the building. The pile has a diameter of 1.0 m and a length of 25.8 m. The soil stratigraphy consists of five layers as summarized in Table 2.

Table 1. Soil profile at the London energy pile site

Layer	Depth (m)	Soil type	Thickness (m)
1	0.0 - 1.5	Made ground	1.5
2	1.5 - 4.0	Sandy gravel	2.5
3	> 4.0	London clay	

Note: Groundwater table is at 3.0 m below ground level (bgl)

Table 2. Soil Profile at the Lausanne energy pile site

Layer	Depth (m)	Description	Thickness (m)
1	0.0 - 5.5	Alluvial soil (A1)	5.5
2	5.5 - 12.0	Alluvial soil (A2)	6.5
3	12.0 - 21.7	Sandy gravelly moraine	9.7
4	21.7 - 25.3	Bottom moraine (till)	3.6
5	> 25.3	Molasse (sandstone)	

Note: Groundwater table is at ground level (0.0 m)

3 NUMERICAL MODEL DESCRIPTION

Numerical modeling was performed using the finite element code PLAXIS 2D-2016. This geotechnical software is capable of modeling fully-coupled THM problems associated with energy piles.

3.1 Material Characteristics

Material parameters shown in Table 3 were considered for the London energy pile. The values were derived based on information given in the literature (Al-Khoury 2008, Bourne-Webb et al. 2009, Thomas & Rees 2009, Rigby-Jones & Milne 2010, Ouyang et al. 2011, Amatya et al. 2012, De Santos et al. 2012, Di Donna 2014, Yavari et al. 2014). The concrete pile was modeled as non-porous elastic material using linear elastic constitutive model (LEM) while the soils were modeled using linear perfectly-plastic Mohr-Coulomb constitutive models (MCM). As for the Lausanne energy pile, the material properties which is not given here due to the length limitation of the paper, were mostly taken from Laloui et al. (2006) with some adjustments, except the hydraulic conductivity of sandstone from Di Donna et al. 2016 and the linear thermal expansion coefficients from Rotta Loria & Laloui 2017. Again, the concrete pile was represented by the LEM. Whereas, the MCM was used for all soils, except for the sandstone bedrock which was represented by the LEM.

3.2 Model Geometry and Boundary Conditions

Axisymmetric models were used for all analyses. As for the London energy pile, the model domain was set at the distance of 50 m (>2L) for the side boundary, and at 75 m (>3L) for the bottom boundary (see Figure 1). These distances were set far enough to minimize or eliminate the boundary effects. The model domain was divided into zones for discretization with very fine meshes at the pile body as well as along the pile-soil interface and around the pile toe. The meshes were gradually made coarser for the zones further away from the pile.

For displacement boundary conditions, a free displacement was allowed at the top. Conversely, both vertical and horizontal displacements were restrained at the bottom (i.e., pinned boundary). Only a vertical displacement was allowed on the left-hand side and right-hand side (i.e., roller boundaries). For hydraulic or groundwater flow boundary conditions, drainage was allowed at the top and right-hand side. A closed flow boundary was assigned along the axisymmetric line and the bottom. For thermal flux boundary conditions, the heat flux was closed (adiabatic condition) at the right-hand side as well as at the left-hand side. A constant temperature of 19.5°C was assigned at the ground surface and the bottom boundary. The initial ground temperature of 19.5°C was also used for the entire model domain. This is the average ground temperature found at the site (Amis et al. 2008).
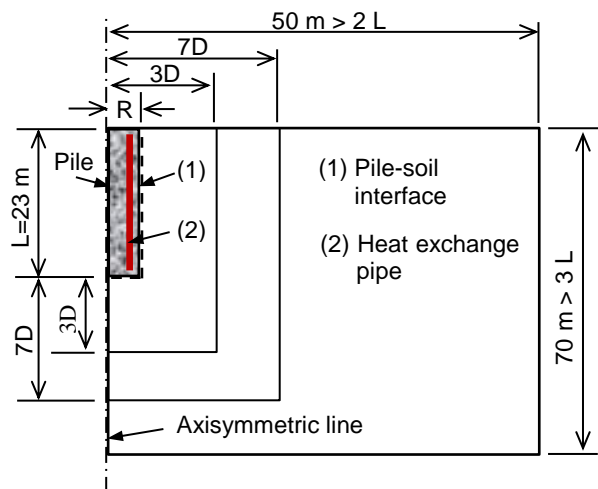

Figure 1. Model geometry for the London energy pile (not to scale)

Regarding the Lausanne energy pile, the width and the height of the model domain were set at 52 m (2L) and 78 m (3L), respectively. The model discretization was done in a similar way with that of the London energy pile. Also, the displacement, groundwater flow, and thermal boundary conditions were the same, except a constant temperature boundary of 13°C was used for the top and bottom boundaries and the initial ground temperature of 13°C was applied for the entire model domain.

3.3 Modeling Procedure

As for the London energy pile, the first step was to establish the initial stress conditions and the initial ground temperature field with the given model parameters and boundary conditions. These were done through the use of the K_o-value and the earth's thermal gradient functions, respectively. The next step was to install the concrete pile (pile was introduced into the models without considering effects of the pile installation). Note that the soil-pile interface elements were used for all analyses with a strength reduction factor of 1.0. This means that the soils and the interface elements have the same strengths. Then, the thermal load in terms of temperature change was applied using the line-based thermal boundary (this implies a circular shell in the axisymmetric models) at the approximate location of the heat exchanger pipes, about 70 mm from the pile shaft. Temperature data recorded in a pile by the thermistor reported in Bourne-Webb et al. (2009) as plotted in Figure 2, was used as the thermal load. The pile was first cooled down from the initial temperature before heating. It should be noted that power interruption caused the drop-down in the temperature during heating at Day 35.

Table 3. Material parameters for analyses of the London energy pile

Parameter	Made ground	Sandy gravel	London clay	Concrete pile
Young's modulus (MPa)	36	140	70	40×10^3
Poisson's ratio	0.3	0.3	0.3	0.15
Cohesion (kPa)	0.5[a]	0.5[a]	20	-
Internal friction angle (°)	33	35	25	-
Dilatancy angle (°)	3	5	0	-
Hor. hydraulic conductivity (m/day)	1	1	1×10^{-5}	-
Vert. hydraulic conductivity (m/day)	1	1	1×10^{-5}	-
Specific heat capacity (kJ/t/°C)	1200	1200	1500	800
Thermal conductivity (kW/m/°C)	2×10^{-3}	2×10^{-3}	1.5×10^{-3}	1.8×10^{-3}
Soil density (t/m³)	1.94	2.04	2.04	2.55
Linear thermal expansion coef. (1/°C)	5×10^{-6}	5×10^{-6}	5×10^{-6}	8.5×10^{-6}

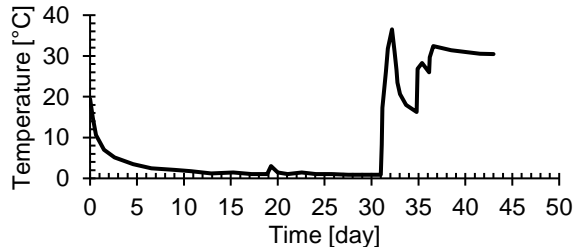[a] small value of c' is used to prevent the numerical complication

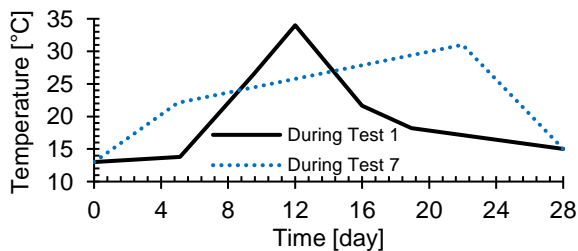Figure 2. Temperature variations with time imposed to the pile for the London energy pile

Figure 3. Temperature variations with time imposed to the pile for the Lausanne pile

Modeling procedure used for the Lausanne energy pile was broadly the same as that of the London energy pile, and thermal loads as shown in Figure 3 were used for Test 1 and Test 7. There was no structure on top of the pile during Test 1 (Laloui et al. 2006, Amatya et al. 2012).

Therefore, the pile was only subjected to thermal load. In Test 7, the building construction had reached the top floor. As a result, the pile was subjected to a mechanical load of about -1300 kN, corresponding to the stress of -1655 kPa before heating and cooling.

3.4 Pile Head Restrained Condition Consideration

Different head restrained conditions (HRC) were considered in the analyses. An unrestrained head condition (URH) was used for the London energy pile because there was no superstructure on top of the pile, except the hydraulic jack and loading frame. For the Lausanne energy pile, the URH was also used for Test 1. However, during Test 7 since the superstructure was already in place, using URH may not represent the field condition. Therefore, varying head restrained conditions were considered to study their effects on pile responses. These include the URH, the fully restrained head (FRH), and partially restrained heads (PRH). The PRH conditions were modeled using fixed-end springs attached to the pile head with varying values of the spring stiffness (EA). i.e., 50, 100 and 200 MPa.

4 RESULTS AND DISCUSSION
4.1 Temperature Distribution

Figure 4 displays the measured and simulated temperature changes with time during cooling-heating cycle for the London energy pile. These values were taken at around mid-length of the pile at locations of the observed borehole

and the anchor pile at 0.5 m and 2.0 m away from the pile center, respectively. Even though at the end of cooling (EOC) the pile temperature was about 0.88°C, the ground temperature at a distance of 0.5 m (≈D) only reduced to 7.9°C from the initial ground temperature of 19.5°C. Moreover, at 2 m away (≈4D), the ground temperature was not affected by the pile cooling and heating, at least, for the test period of about 43 days. Since there is no groundwater flow and the hydraulic conductivity of the clay is very low in the order of 1x10^{-5} m/day, the heat transfer in the ground is due only to conduction. As shown in Figure 4, the measured (using thermistors and optical fiber sensors, OFS, taken from Bourne-Webb et al. 2009) and simulated temperature values agree well. The numerical model, therefore, was able to predict the temperature distribution in the surrounding ground accurately.
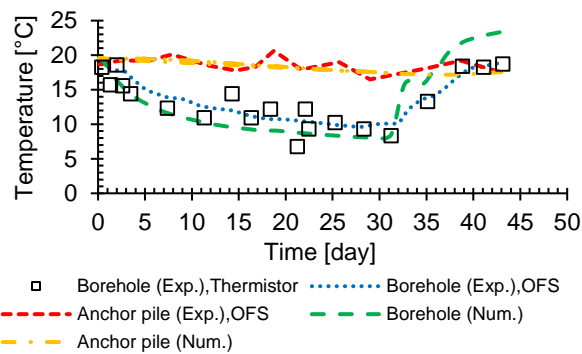
Figure 4. Temperature changes over time during a cooling-heating cycle at the locations of the observed borehole and the anchor pile (London energy pile).

4.2   Pile Vertical Displacement

Pile vertical displacements along the pile length for the London energy pile are shown in Figure 5. The mechanical load (M) caused the contraction in the entire pile, and downward displacements were induced with a maximum value of -3.1 mm at the pile head and a minimum value of -1.6 mm at the pile toe. Cooling caused the pile to contract even further, but unlike the contraction induced by the M load, the thermally induced contraction occurred with respect to the location of the neutral plane (NP) where the pile did not move. During cooling, the portion above the NP moved down whereas the portion below it moved up. These resulted in further head displacement to -6.2 mm at the end of cooling (EOC) but reduced the toe displacement to -0.9 mm. When the pile was heated, from the EOC period, about one half of the pile moved up while other half moved down. These happened because heating caused the pile to expand about the NP.

The Lausanne energy pile tests show similar responses in which the pile expanded and contracted around the NP when heated and cooled. Figure 6 shows the pile vertical displacement profiles induced by the thermal load (T) for Test 1 with the pile head displacement of 3.4 mm at the end of heating (EOH) and 1 mm at the EOC. Figure 7 displays the pile vertical displacements for Test 7. As can

be seen in the figure, the head restrained conditions (HRC) significantly influenced the pile head displacements with values ranging from 2 mm for the unrestrained head (URH) to zero for the fully restrained head (FRH) and somewhere in between for the partially restrained head (PRH), depending on the restrained stiffness. Note that the NP locations also moved upwards for the stiffer pile head restraints. Moreover, because the pile toe is socketed into sandstone bedrock, it hardly moved down at all at the EOH (only -0.4 mm).
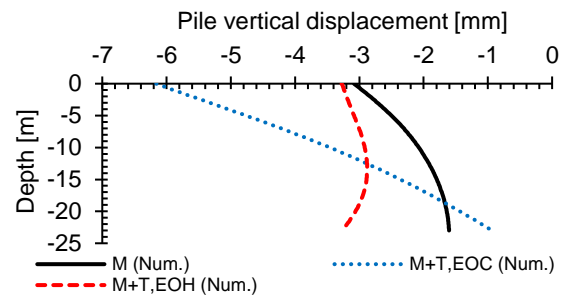

Figure 5. Pile vertical displacement profiles at the end of cooling and heating (London energy pile)
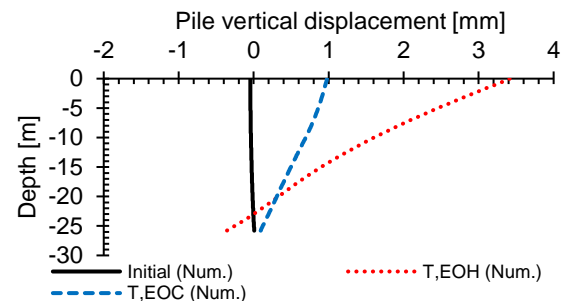

Figure 6. Pile vertical displacement profiles at the end of cooling and heating (Lausanne energy pile: Test 1)

As a result of the cooling-heating or heating-cooling cycle, the pile head moved up and down following the rise and fall of the temperature. As shown in Figure 8 for the London energy pile and Figure 9 for the Lausanne energy pile Test 1, the computed and measured pile head movements (taken from Bourne-Webb et al. 2009 and Laloui et al. 2006, respectively) agree quite well which means that the numerical simulations performed as desired. In the London energy pile, the maximum predicted settlement of the pile head was -6.2 mm (≈1.2%D) at the EOC in comparison with -5.5 mm from the experiment. Likewise, the pile head uplift measured using different devices at the EOH for Test 1 of Lausanne energy pile varied from 3.4 mm (Levelling), 3.6 mm (Optical fibers) to 4.4 mm (Extensometers), compared with the predicted value of 3.4 mm (≈0.6%D).
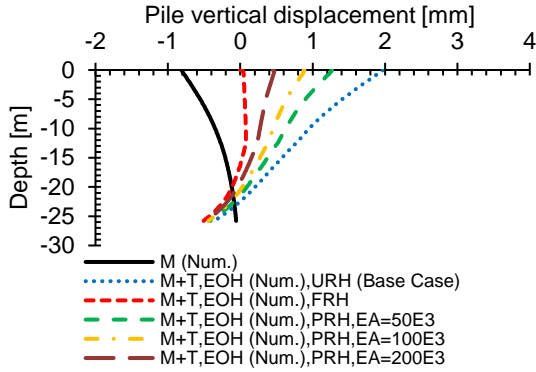
Figure 7. Pile vertical displacement profiles at the end of heating (Lausanne energy pile: Test 7)
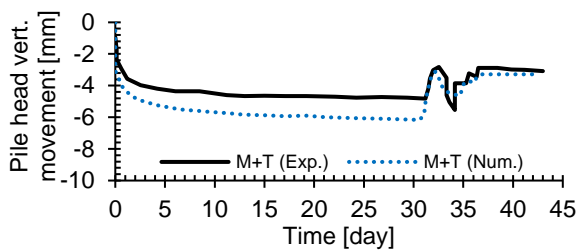

Figure 8. Pile head movement during a cooling-heating cycle (London energy pile)
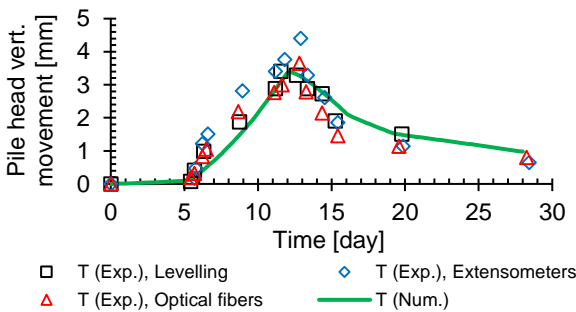

Figure 9. Pile head movement during a heating-cooling cycle (Lausanne energy pile: Test 1)

4.3 Pile Axial Strain

Axial strain profiles of the pile in responses to mechanical and thermo-mechanical loads are illustrated in Figures 10(a) and 10(b) for the London energy pile. Note that the axial strains caused by only mechanical load (M) were plotted in all figures for reference purposes. In Figure 10(a), the thermal cooling induced contractive strains (negative) in the pile, and therefore, added to the contractive strains caused by the M load. As a result, the strain profiles of a combined effect of mechanical and thermal loads at the end of cooling (M+T, EOC) shifted to the left-hand side. The reverse responses occurred during heating in which the pile expanded, resulting in expansive strains (positive) in the pile and reducing the mechanically induced compressive strains. Therefore, the strain profiles induced by the thermo-mechanical load at the end of heating (M+T,

EOH) shifted to the right-hand side, leading to expansive strains at the bottom half of the pile as shown in Figure 10(b). It can be seen that the mechanical strains from numerical and experimental data agree quite well, except the upper 5 m of the pile. The reason for this difference may be due to the pile restrained conditions that may not be appropriately represent by the numerical model or it may be because of the measurement variation. The strains caused by the thermo-mechanical load at the end of cooling (M+T, EOC) and heating (M+T, EOH) are also comparable, and similar patterns were observed for both simulations and experiment (from Amatya et al. 2012).
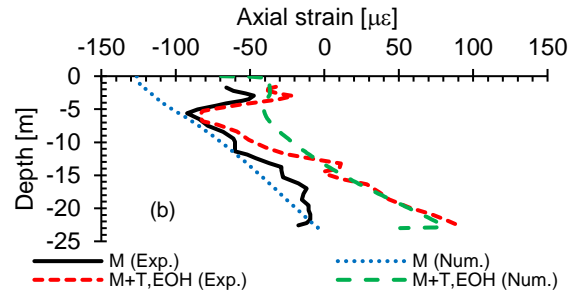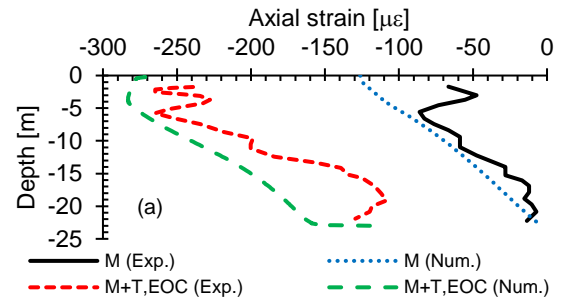

Figure 10. Axial strain profiles (a) at the end of cooling (b) at the end of heating (London energy pile)

As for the Lausanne energy pile, Figure 11 compares the expansive axial strains induced by the thermal load (T) alone between the results of numerical simulations and experiment at the EOH and at the EOC in Test 1. Again, the values are comparable with similar patterns of strain profiles, although the model slightly under-predicted the strains at the lower part of the pile at the EOH. This may be due to the assumption that there was no stiffness reduction of the sandstone right underneath the pile toe in the model. In the field, however, this stiffness may be less because of the imperfection of borehole base cleaning before the concrete was poured. Lower stiffness resulted in higher strains. The axial strains induced by the M and M+T loads in Test 7 at the EOH and EOC are shown in Figure 11. The experimental data were taken from Amatya et al. (2012). It can be seen that the mechanically induced strains are in good agreement with the measured data, especially at the lower half of the pile. When the pile was heated, T heating load, expansive strains were induced whereas the M load produced compressive strains. The combined thermo-mechanical axial strains at the EOH

(M+T, EOH) were seen to vary with different pile head restraints. From Figure 12, it seems that the measured strain profile lies within the simulated ones and more importantly the models with partially restrained head conditions (PRH) better depicted the measured values.
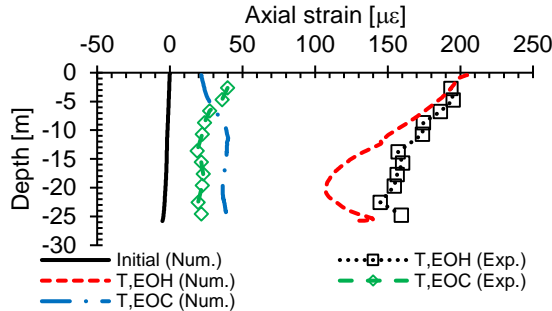

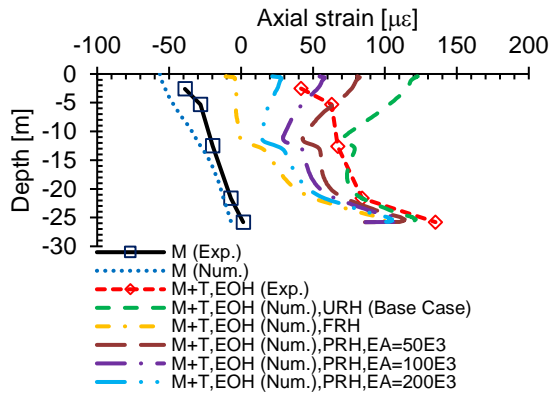Figure 11. Axial strain profiles at the end of heating and cooling (Lausanne energy pile: Test 1)

Figure 12. Axial strain profiles at the end of heating (Lausanne energy pile: Test 7)

4.4   Pile Axial Load

Results from the London energy pile analyses are shown in Figure 13(a) and 13(b). The axial compressive stresses (negative) were induced in the pile when the mechanical load (M) of -1200 kN was applied to the pile head. This load then transferred to the surrounding soils through the shaft friction and gradually reduced, reaching -145 kN at the pile toe. The predicted load transfer profile closely resembles the field data reported in Bourne-Webb et al. (2009) using vibrating strain gauges (VWSG) and optical fiber sensors (OFS). It appears from numerical results that, at the EOC, the axial load profile was hardly affected by cooling. Consequently, the thermo-mechanically induced load profile at the EOC (M+T, EOC) was increased and reduced marginally at the top and bottom halves, respectively, as shown in Figure 13(a). However, experimental data show that there were considerable decreases in the axial loads at the lower half of the pile, resulting in the maximum tensile loads of about 122 kN (VWSG) and about 480 kN (OFS) for $\Delta T \approx -18.6°C$. A discrepancy in the values between different measuring devices are observed.

Nonetheless, this means that cooling, in fact, induced the tensile stresses or loads in the pile. The numerical model could not efficiently capture that behavior. During heating, the axial compressive stresses or loads were generated. These thermally induced compressive loads, with the maximum simulated value of -436 kN for $\Delta T \approx +11°C$, were added to the mechanically induced ones (M+T, EOH) as shown in Figure 13(b) in which the maximum of about -1300 kN was resulted and located at about 5 m bgl. In comparison with the measurements, the numerical model under-predicted the axial loads in the top half considerably, especially at about 5 m depth. Again, this may be due to the difference between pile restrained conditions in the model and in the field, resulting from the assumptions of the soil stiffness and the head restrained condition. In the bottom half, however, both simulated and measured values are more comparable.
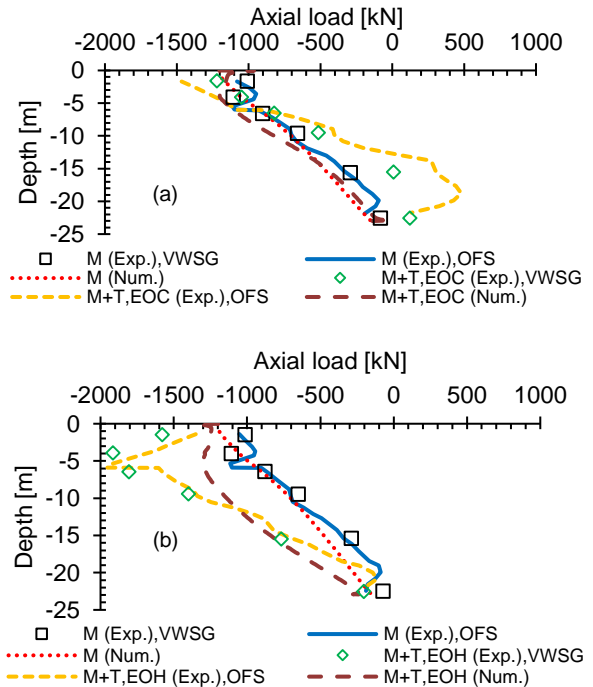

Figure 13. Axial load profiles (a) at the end of cooling (b) at the end of heating (London energy pile)

The thermally induced axial load profile for the Lausanne energy pile Test 1 is given in Figure 14. The numerical results agree well with the experiment (from Amatya et al. 2012) at the EOH (T, EOH), especially in the upper part of the pile. The maximum predicted thermally induced load was about -2700 kN for $\Delta T=+21°C$. In Test 7, the pile was subjected to both thermal and mechanical loads. When the pile was heated, $\Delta T=+18°C$, the thermally induced compressive loads up to -2750 kN was generated in the case of using the PRH with EA=100 MPa, which is approximately twice the applied M load of -1300 kN. The combined effects of these loads were displayed in Figure 15 together with results using other restrained conditions. As expected, the simulations with different head restraints

gave different axial load profiles. It seems that the model using the PRH with EA=100 MPa captured the field response very well with the maximum simulated thermo-mechanical load at the EOH (M+T, EOH) of -3600 kN, comparing with -3640 kN from the experiment (from Amatya et al. 2012). Higher spring stiffness generated higher axial loads in the pile. The smallest axial load was produced by the URH case while the highest was by the FRH case because the pile head could not move, leading to the generation of higher thermal stresses. These numerical results show that it is vital to consider appropriate pile restrained conditions when examining the responses of energy piles subjected to thermo-mechanical loading.
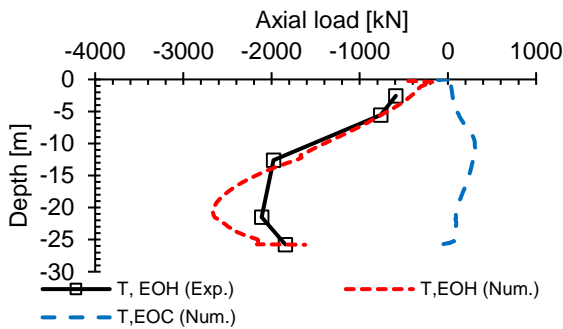
Axial load [kN]

Figure 14. Axial load profiles at the end of heating and cooling (Lausanne energy pile: Test 1)
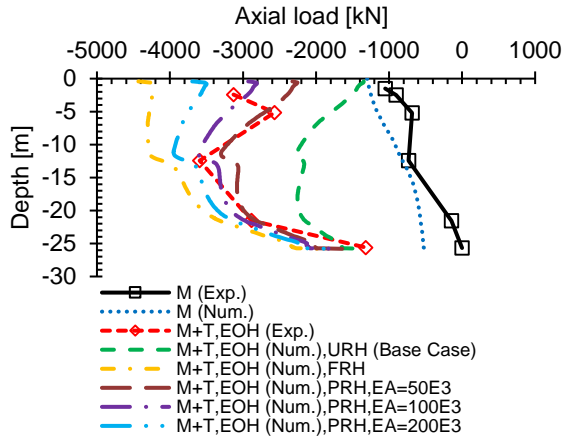
Axial load [kN]

Figure 15. Axial load profiles at the end of heating (Lausanne energy pile: Test 7)

4.5   Mobilized Shaft Friction

Energy piles cannot freely expand or contract when heated or cooled partly due to shaft friction developed along the pile-soil interface. Figure 16(a) and 16(b) show the mobilized shaft friction induced by the M, M+T at the EOC, and M+T at the EOH for the London energy pile. The M load generated all positive (acting upwards) shaft friction with the maximum value of 42 kPa, which is comparable to the measured value of 50 kPa (VWSG) and 35 kPa (OFS). At the EOC, the mobilized shaft friction increased in the

upper 19 m (above the NP), except a reduction near the ground surface. Below 19 m bgl, the values were more or less unchanged. At the EOH, the mobilized shaft friction reduced in the top half (above the NP), reaching -26 kPa (acting downwards). In other words, negative shaft friction was developed. In the bottom half, however, there was an increase in the mobilized shaft friction. Even though the numerical predicted and measured values are not precisely matched, the numerical models provided similar trends of the mobilized shaft friction.

Figure 17 shows the mobilized shaft friction at the EOH and EOC in Test 1. As seen in the graph, the measured and simulated profiles at the EOH are comparable and the negative shaft friction of -58 kPa was induced in the top part of the pile above the NP. The opposite is true for the bottom part with the shaft friction of up to 80 kPa. Similar responses occurred in Test 7. Furthermore, different pile head restraints produced different shaft friction responses in which, in general, the simulations agree well with the experiment (see Figure 18).

Mobilized shaft friction [kPa]
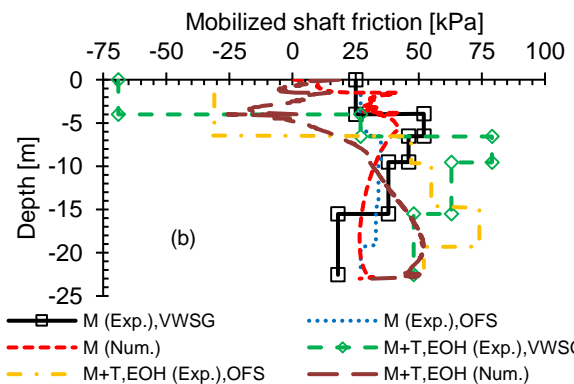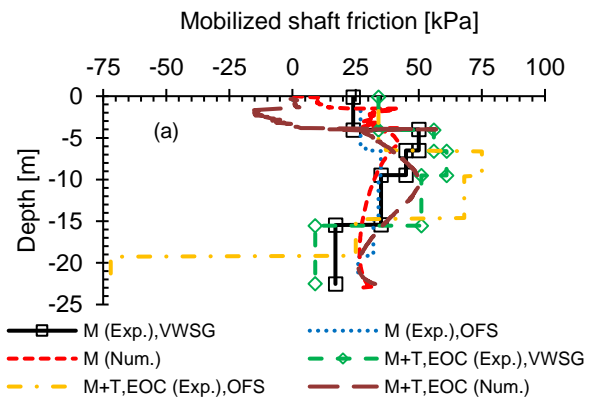

Mobilized shaft friction [kPa]

Figure 16. Mobilized shaft friction (a) at the end of cooling (b) at the end of heating (London energy pile)
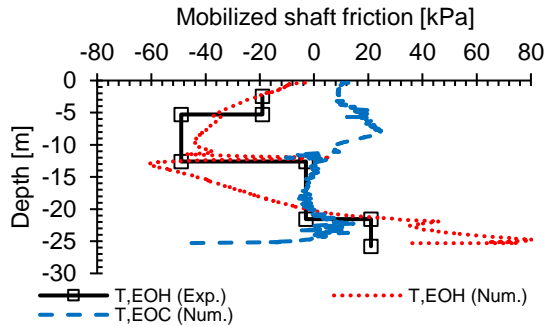
Figure 17. Mobilized shaft friction at the end of heating and cooling (Lausanne energy pile: Test 1)
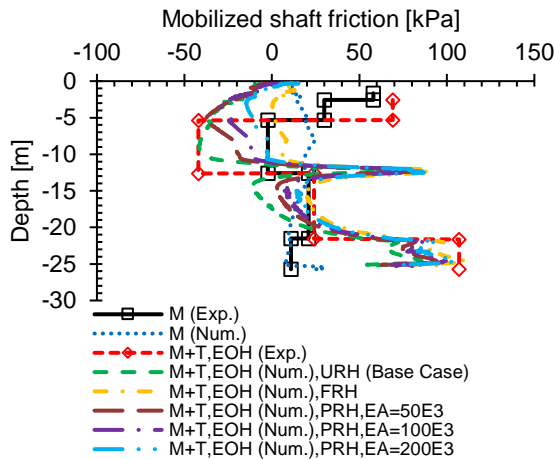

Figure 18. Mobilized shaft friction at the end of heating (Lausanne energy pile: Test 7)

5   CONCLUSIONS

The behavior of energy piles subjected to thermal and thermo-mechanical loadings have been examined numerically in this paper through the use of fully-coupled THM finite element models. The simulations were able to capture general responses of energy piles quite well in comparison with experimental data observed for the two case studies conducted in the U.K and Switzerland. The models, however, seem to predict the responses of the piles during heating better than during cooling. Based on numerical results, it can be said that temperature changes in the piles have significant effects on their stresses and strains. In general, heating causes the piles to expand, resulting in expansive strains. If the piles cannot expand freely due to shaft friction and end restraints, thermal compressive stresses will be generated in addition to the mechanically induced ones. Cooling causes reverse effects but to a lesser extent. These thermally induced stresses should be considered in the energy pile design. Also, heating produces uplift of the pile head while cooling causes settlement. The heating-cooling cycle of the pile also affects the surrounding ground temperature to some distances. The mobilized shaft friction along the pile length is also affected by the temperature changes to some extent. When model the energy piles, it is essential to consider appropriate head restrained conditions to capture the correct pile responses.

6   REFERENCES

Al-Khoury, R. 2008. Computational Modeling of Shallow Geothermal Systems, CRC Press, Taylor & Francis Group, Boca Raton, Florida, FL, USA.

Amatya, B.L., Soga, K., Bourne-Webb, P.J., Amis, T., and Laloui, L. 2012. Thermo-mechanical behaviour of energy piles. Géotechnique, **62**(6): 503–519.

Amis, T., Bourne-Webb, P., Davidson, C., Amatya, B., and Soga, K. 2008. The effects of heating and cooling energy piles under working load at Lambeth College, UK. Proceedings of the 33rd Annual and 11th Int. Conference on Deep Foundations.

Bourne-Webb, P.J., Amatya, B., Soga, K., Amis, T., Davidson, C., and Payne, P. 2009. Energy pile test at Lambeth College, London: geotechnical and thermodynamic aspects of pile response to heat cycles. Géotechnique, **59**(3): 237–248.

Brandl, H. 2006. Energy foundations and other thermo-active ground structures. Géotechnique, **56**(2): 81–122.

Di Donna, A. 2014. Thermo-mechanical aspects of energy piles. Ph.D Thesis, Swiss Institute of Technology in Lausanne, Switzerland.

Di Donna, A., Rotta Loria, A.F., and Laloui, L. 2016. Numerical study of the response of a group of energy piles under different combinations of thermo-mechanical loads. Computers and Geotechnics, **72**: 126–142.

Laloui, L., Nuth, M., and Vulliet, L. 2006. Experimental and numerical investigations of the behaviour of a heat exchanger pile. International Journal for Numerical and Analytical Methods in Geomechanics, **30**(8): 763–781.

Ouyang, Y; Soga, K; Leung, Y.. 2011. Numerical Back-analysis of Energy Pile Test at Lambeth College, London. *In* Geo-Frontiers: 440–449.

Rigby-Jones, J.; and Milne, C. 2010. PLAXIS analysis of a basement excavation in central London. PLAXIS Bulletin, Autumn Issue 2010: 14–17.

Rotta Loria, A.F., and and Laloui, L. 2017. Thermally induced group effects among energy piles. Géotechnique, **67**(5): 374–393.

De Santos, C., Ledesma, A., and Gens, A. 2012. Backanalysis of measured movements in ageing tunnels. 7th International Symposium on Geotechnical Aspects of Underground Construction in Soft Ground: 223–229.

Thomas, H.R.. and, and Rees, S.W. 2009. Measured and simulated heat transfer to foundation soils. Géotechnique, **59**(4): 365–375.

Yavari, N., Tang, A.M., Pereira, J.-M., and Hassen, G. 2014. A simple method for numerical modelling of mechanical behaviour of an energy pile. Géotechnique Letters, **4**(2): 119–124.